

# Concentration-dependent mobility in organic field-effect transistors probed by infrared spectromicroscopy of the charge density profile

A. D. Meyertholen, Z. Q. Li, D. N. Basov, and M. M. Fogler

*Department of Physics, University of California San Diego, La Jolla, 9500 Gilman Drive, California 92093*

M. C. Martin

*Advanced Light Source Division, Lawrence Berkeley National Laboratory*

G. M. Wang, A. S. Dhoot, D. Moses, and A. J. Heeger

*Institute for Polymers and Organic Solids and Mitsubishi Chemical Center for Advanced Materials, University of California, Santa Barbara*

(Dated: August 25, 2017)

We show that infrared imaging of the charge density profile in organic field-effect transistors (FETs) can probe transport characteristics which are difficult to access by conventional contact-based measurements. Specifically, we carry out experiments and modeling of infrared spectromicroscopy of poly(3-hexylthiophene) (P3HT) FETs in which charge injection is affected by a relatively low resistance of the gate insulators. We conclude that the mobility of P3HT has a power-law density dependence, which is consistent with the activated transport in disorder-induced tails of the density of states.

Transport characteristics of organic semiconductors are important for optimizing the performance of organic FETs. Due to substantial disorder, polaronic, and interaction effects, transport mechanisms in organics are complicated and standard model assumptions used for inorganic devices may be unrealistic. For example, the canonical model of the FET [1] assumes that the mobility  $\mu$  is independent of the areal carrier density  $N$  in the accumulation (or inversion) layer, while theoretical and experimental investigations of organic conductors point to the contrary [2, 3, 4, 5]. Unfortunately, the extraction of mobility from traditional transport measurements is complicated by the nonlinearity of the contact resistance, which may obscure the intrinsic mobility of the organic semiconductor [6, 7].

Recently, we have reported a direct imaging of the charge distribution in the accumulation layer of organic FETs using infrared (IR) spectromicroscopy [8]. In this Letter we show that this contactless technique is complementary to traditional DC transport measurements. Specifically, the carrier density profile in the conducting channel obtained from the IR scans can be used to extract the intrinsic behavior of the density-dependent mobility, avoiding artifacts due to the contacts.

As a case study, we investigated P3HT-based FETs in which an inhomogeneous charge density profile was formed due to a non-negligible leakage current through the gate dielectrics. Below we show that the idealized model [1] fails to correctly account for the charge density distribution observed in these FETs. Instead, we find a good agreement with the model of a density-dependent mobility,

$$\mu = \text{const} \times N^\beta, \quad \beta = (E_*/k_B T) - 1 \geq 0, \quad (1)$$

which is derived theoretically below assuming transport

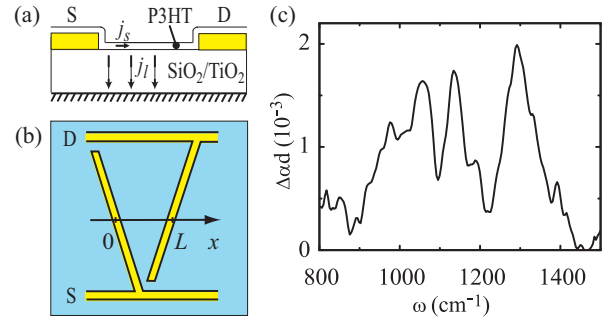


FIG. 1: (a) FET schematics (b) A sketch of the V-shaped electrodes between which the IR scans were taken. (c) The voltage-induced absorption spectrum  $\delta a d$  of one of the FET devices studied. The sharp absorption peaks are the IR-active vibrational modes of P3HT.

is activated and the density of states has an exponential tail with the characteristic energy width  $E_*$ . Since  $E_*$  depends on disorder, exponent  $\beta$  is not known precisely. From the fits to our IR spectromicroscopy data we find  $1 < \beta < 4$  at temperature  $T = 300$  K, where all the measurements are done. This implies  $E_* \sim 0.1$  eV, which agrees with other experiments on P3HT [9]. The power-law behavior (1) has been previously observed both in P3HT [5] and in other organic conductors [2]. Thus, it is common to this class of materials.

Let us proceed to the description of our experiment. The structure of the FETs is shown in Fig. 1(a). In these bottom-contacted devices, source and drain Au electrodes were deposited on  $\text{SiO}_2/\text{TiO}_2/\text{n-Si}$  substrates followed by the spin coating of a 4–6 nm thick P3HT film,

which served as the electronically active material. To examine length scales associated with charge injection, we fabricated devices with a V-shaped electrode pattern [Fig. 1(b)] where the electrode separation varied from 0.01 mm at one side to 4 mm at the other. To image the injected charges we have employed the IR spectro-microscopy, which involved scanning a focused IR beam 50–100  $\mu\text{m}$  in diameter across the region between the V-shaped electrodes and monitoring the changes in the P3HT absorption spectrum at a given gate voltage [8].

The spectroscopic “fingerprints” of the injected charges in P3HT are the IR-active vibrational modes [Fig. 1(c)] and the polaron band (a broad absorption maximum at  $\omega \sim 3500 \text{ cm}^{-1}$ , cf. Fig. 2 of Ref. [8]). From the oscillator strength of the former, we computed the gate-induced charge density  $N(x)$  as a function of the distance  $x$  from the source electrode. (These results agreed within the experimental accuracy with  $N(x)$  computed from the polaron band spectra, see Ref. [8] for details.) In Fig. 2, we plot  $N(x)$  normalized to its value at  $x = 0$  for three representative devices. Our main result is that the injected charge density decays with the distance from the source and vanishes at  $x \sim 800 \mu\text{m}$ . Below we show that the spatial variation of the charge density contains valuable information on the  $N$ -dependence of the mobility in accumulation layers of organic FET.

Indeed, in the experiment a non-negligible leakage current  $j_l$  through the dielectric [10] was detected. The corresponding effective resistivity of the dielectric layer  $\rho_l = V/j_l$  was a function of  $V$ , the voltage difference between the polymer and the gate. However,  $\rho_l \approx \text{const}$  was observed [10] at  $V > 5 \text{ V}$  and, for simplicity, we assume this to be the case. In the gradual-channel approximation suitable for our FETs we obtain the balance of surface ( $\mathbf{j}_s$ ) and leakage ( $j_l$ ) currents as follows:

$$-\nabla \mathbf{j}_s = \nabla(\sigma \nabla V) = V/\rho_l. \quad (2)$$

For the sheet conductivity  $\sigma$  we adopt the form  $\sigma = \sigma_a + \sigma_r$ , where  $\sigma_a$  and  $\sigma_r$  are the sheet conductivities of the accumulation layer and the residual mobile charges, respectively. Initially, let us make the conventional assumptions that (i)  $\mu \equiv \sigma_a/N = \text{const}$  (ii)  $\sigma_r \ll \sigma_a$ , and (iii)  $V = eN/C$ , where  $C = \text{const}$  is the capacitance per unit area ( $C \approx 0.14 \mu\text{F}/\text{cm}^2$  in our FETs). This entails

$$\nabla(N \nabla N) \simeq N/(e\mu\rho_l). \quad (3)$$

Since the characteristic length of charge inhomogeneity is smaller than the lateral extension of the source and drain electrodes in the V-shaped region [Fig. 1(b)], it is permissible to treat them as infinite metallic half-planes,  $x < 0$  and  $x > L$ , respectively. In this case, all variables depend only on  $x \in (0, L)$ . Suppose first that  $L$  is very large (the source and drain are far apart), then the physically relevant solution of Eq. (3) is

$$N(x) \simeq N(0)[1 - (x/x_*)]^2, \quad x < x_* \equiv \sqrt{6\sigma(0)\rho_l}. \quad (4)$$

Interestingly, it predicts that the charge injection has a definite cutoff length  $x_*$ . This occurs because of the quadratic nonlinearity of Eq. (3). Treating  $x_*$  as an adjustable parameter, we plot Eq. (4) in Fig. 2 (the curves labeled  $\beta = 0$ ). Alternatively, we can estimate  $x_*$  based on  $\sigma$  and  $\rho_l$  deduced from the DC transport measurements [8, 10],  $\sigma \sim 10^{-7} \Omega^{-1}$  and  $\rho_l \sim 10^5 \Omega \text{ cm}^2$ , which yields  $x_* \sim 2500 \mu\text{m}$ . Comparing with Fig. 2, we see that the observed  $x_*$  is significantly smaller. Furthermore, instead of a more gradual decrease in the conventional theory, in experimental data  $N(x)$  exhibits an abrupt drop. This suggests that the degree of nonlinearity of the actual current balance equation (2) is higher than quadratic.

The field-dependence of  $\mu$  is probably not the main source of this effect because we study P3HT of a rather high mobility  $\mu = 0.05\text{--}0.12 \text{ cm}^2/\text{Vs}$ , where non-Ohmic behavior is not as pronounced as in low-mobility organics [3, 4, 5, 6], and also because  $T$  was relatively high [11]. On the other hand, there is a natural reason for the  $N$ -dependence of  $\mu$  [conveyed by Eq. (1)]. At densities we deal with,  $N < 10^{13} \text{ cm}^{-2}$ , the system approaches the insulator-to-metal transition region [12]. The chemical potential  $\zeta$  presumably resides in the density-of-states tail of disorder-induced traps but at temperatures of interest such traps are shallow (a few  $k_B T$  deep). Therefore, transport is dominated by the activation of carriers to either the mobility edge or the so-called transport energy level [3, 4] and it is characterized by a modestly large activation energy  $|\zeta|$ , i.e.,  $\sigma_a \propto \exp(\zeta/k_B T)$  (the mobility edge is taken to be the energy reference point) [13]. Because of this exponential relation between the conductivity and  $\zeta$ , the dependence of  $\zeta$  on  $N$  is amplified in  $\sigma_a$ , producing the sought nonlinear effect.

It is possible to express  $\sigma_a$  directly as a function of  $N$  if the density of states  $g(E)$  is known. In conducting polymers  $g(E)$  is often modeled by Gaussian or exponential forms [3], which are observed experimentally [9]. In either case we obtain  $N(\zeta) = \int dE g(E) f(E, \zeta) \simeq N_t \exp(\zeta/E_*)$ , up to logarithmic factors. Here  $f(E, \zeta)$  is the Fermi-Dirac distribution function,  $E_* > k_B T$  is the characteristic energy width of the band tail, and  $N_t$  is the total number of states per unit area in this tail. We see that  $\zeta \simeq E_* \ln(N/N_t)$ , leading to  $\sigma_a \simeq \sigma_*(N/N_t)^{\beta+1}$  with  $\beta + 1 = E_*/k_B T$ . Consequently, the mobility is  $\mu(N) \equiv \sigma_a/eN \propto N^\beta$ , in agreement with Eq. (1). We note that a nearly identical  $\mu(N)$  dependence also follows from the hopping transport model [3, 4]. Equation (1) was also postulated in Ref. [7]. Substituting  $\sigma \propto N^{\beta+1}$  into Eq. (2) but still neglecting  $\sigma_r$ , we obtain

$$N \simeq N(0) \left(1 - \frac{x}{x_*}\right)^{\frac{2}{\beta+1}}, \quad x_* = \frac{\sqrt{2(\beta+3)\sigma(0)\rho_l}}{\beta+1} \quad (5)$$

with Eq. (4) being recovered for  $\beta = 0$ . Three representative curves computed according to Eq. (5) are plotted in each panel of Fig. 2. Clearly, for all of the three

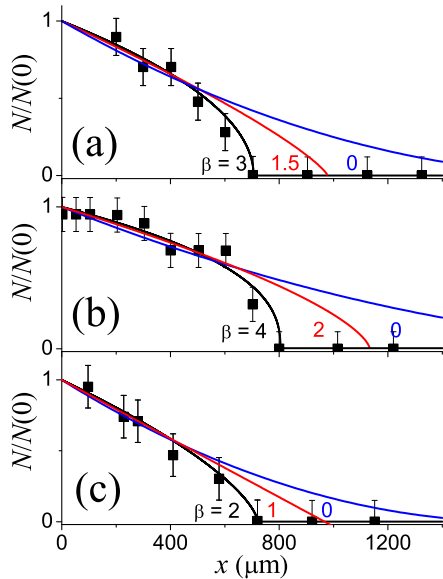


FIG. 2: Charge density profiles measured by the IR spectroscopy in three nominally similar devices. The solid lines are theoretical fits (see text).

FETs studied, one can find  $\beta$ s somewhere in the range  $1 < \beta < 4$  which give a significantly better fit to experiment than  $\beta = 0$ , both in the functional form and in the value of  $x_*$ . Apparently, Eq. (1) is more suitable for modeling the charge injection profile in a “leaky” FET.

For future reference we mention that a refinement of the model including the residual conductivity,

$$\sigma = \sigma_*(N/N_t)^{\beta+1} + \sigma_r. \quad (6)$$

predicts the injected charge density profile of the form

$$\frac{x}{x_*} = -\sqrt{u+a} + \frac{2\sqrt{a}}{\beta+3} \ln \frac{\sqrt{u+a} + \sqrt{a}}{\sqrt{u+a} - \sqrt{a}} + \text{const}, \quad (7)$$

$$u \equiv [N(x)/N(0)]^{\beta+1}, \quad a \equiv (\beta+3)\sigma_r/[2\sigma_a(0)]. \quad (8)$$

Accordingly,  $N(x) \propto \exp(-x/\sqrt{\sigma_r \rho l})$  at  $x > x_*$ , i.e., it has the exponential decay instead of the abrupt threshold predicted by Eq. (5). However, since  $\sigma_r/\sigma(0) \sim 10^{-4}$ – $10^{-3}$  (the on-off ratio) [10], the pre-exponential factor of this tail is very small, producing apparently no signature in our experiment, see Fig. 2.

Finally, let us also discuss the  $L < x_*$  case where the injected charge is able to reach the drain (as in SiO<sub>2</sub> devices we studied previously [8]). Here  $N(x)$  depends on the bias  $V_{SD} \equiv V(0) - V(L)$ . Also, the right-hand side of Eq. (2) can be set to zero because we can normally neglect the leakage current  $j_l$  compared to the source-drain current  $j_s$ . Equation (2) remains solvable [14] and

yields the algebraic equation for  $N(x)$ ,

$$\frac{\sigma_* N_t}{\beta+2} \left(\frac{N}{N_t}\right)^{\beta+2} + \sigma_r N = \frac{C j_s}{e} (x_p - x), \quad (9)$$

where  $x_p$  is the integration constant. At  $V(L) \rightarrow 0$ , we have  $x_p \rightarrow L$  and, except very near the drain, the first term on the left-hand side dominates. In this case the charge profile is very similar to that of the injection case, Eq. (5), except  $x_*$  is replaced by  $L$  and the power-law exponent  $2/(\beta+2)$  is changed to a smaller number  $1/(\beta+2)$ . Although we were not able to verify this formula by our technique (in part, due to a finite spatial resolution  $\sim 100 \mu\text{m}$ ) we note that Bürgi *et al.* [5] have studied this regime in similar FET devices using scanning potentiometry. These authors were able to fit their data to the formula obtained by setting  $\sigma_r = 0$  and  $\beta = 1$  in our Eq. (9) [15].

In conclusion, when the charge profile in the organic semiconductor is strongly inhomogeneous, as in the charge injection [8] or the current saturation [5] regimes, its modeling should include the density dependence of the carrier mobility. Our experiment is consistent with the power law (1), which has a natural physical motivation. Our measurements and the method of analysis are free from problems introduced by the contact resistance.

Work at UCSB was supported by the NSF grant DMR-0602280. The UCSD team was supported by the NSF grant ECS-0438018 and UCSD ACS. We thank D. Natelson for comments on the manuscript.

- 
- [1] S. M. Sze, *Physics of Semiconductor Devices* (Wiley, New York, 1981).
  - [2] A. R. Brown, C. P. Jaret, D. M. de Leeuw, and M. Matters, *Synth. Met.* **88**, 37 (1997).
  - [3] M. C. J. M. Vissenberg and M. Matters, *Phys. Rev. B* **57**, 12964 (1998).
  - [4] W. F. Pasveer *et al.*, *Phys. Rev. Lett.* **94**, 206601 (2005).
  - [5] L. Bürgi, H. Sirringhaus, and R. H. Friend, *J. Appl. Phys.* **80**, 2913 (2002); L. Bürgi *et al.*, *Synth. Met.* **146**, 297 (2004).
  - [6] B. H. Hamadani and D. Natelson, *J. Appl. Phys.* **95**, 1227 (2004); **97**, 064508 (2005).
  - [7] D. Natali, L. Fumagalli, and M. Sampietro, *J. Appl. Phys.* **101**, 014501 (2007).
  - [8] Z. Q. Li, G. M. Wang, N. Sai, D. Moses, M. C. Martin, M. Di Ventra, A. J. Heeger, and D. N. Basov, *Nano Lett.* **6**, 224 (2006).
  - [9] O. Tal *et al.*, *Phys. Rev. Lett.* **95**, 256405 (2005).
  - [10] G. Wang *et al.*, *J. Appl. Phys.* **95**, 316 (2004).
  - [11] No significant field-dependence of  $\mu$  was found experimentally at such temperature [5, 10]. The nonlinearity of the contact resistance can still be significant [5]; however, it has no effect on our contactless measurements.
  - [12] A. S. Dhoot, G. M. Wang, D. Moses, and A. J. Heeger, *Phys. Rev. Lett.* **96**, 246403 (2006).

- [13] By means of repeated capture and release from shallow traps, charge carriers in our experiment travel macroscopic distance (almost a mm) away from injecting electrodes and the decay of  $N(x)$  is detected chiefly because we intentionally work with a large-area FET with a non-negligible leakage current.
- [14] Deep in the current saturation regime (where  $V(0)$  and  $V(L)$  are of opposite sign) one cannot treat the problem as one-dimensional, and  $\sigma_r$  becomes position dependent, see, e.g., Ref. [2]. We do not consider this case here.
- [15] In order to obtain this fit Bürgi *et al.* had to shift all their data by 2 V, a significant fraction of the total  $V_{SD} = 8$  V. They argued that such a shift can be viewed as a way to account for residual carriers. We think that a more consistent approach is in terms of a finite  $\sigma_r$ .